



Tuning frequency band gaps of tensegrity mass-spring chains with local and global prestress

Ada Amendola^{a,*}, Anastasiia Krushynska^b, Chiara Daraio^c, Nicola M. Pugno^{d,e,f},
Fernando Fraternali^a

^a Department of Civil Engineering, University of Salerno, Via Giovanni Paolo II, 132, Fisciano SA 84084, Italy

^b Department of Physics, University of Turin, Via P. Guria, 1, Turin 10125, Italy

^c Engineering and Applied Science, California Institute of Technology, Pasadena, CA 91125, USA

^d Laboratory of Bio-Inspired and Graphene Nanomechanics, Department of Civil, Environmental and Mechanical Engineering, University of Trento, Via Mesiano, 77, Trento 38123, Italy

^e School of Engineering and Materials Science, Queen Mary University of London, Mile End Road, London E1 4NS, UK

^f Ket Labs, Edoardo Amaldi Foundation, Italian Space Agency, Via del Politecnico snc, Rome 00133, Italy

ARTICLE INFO

Article history:

Received 30 January 2018

Revised 23 June 2018

Available online 18 August 2018

Keywords:

Tensegrity lattice

Band gaps

Prestress

Wave attenuation

Monoatomic

Biatomic

Tunability

ABSTRACT

This work studies the acoustic band structure of tensegrity mass-spring chains, and the possibility to tune the dispersion relation of such systems by suitably varying local and global prestress variables. Building on established results of the Bloch–Floquet theory, the paper first investigates the linearized response of chains composed of tensegrity units and lumped masses, which undergo small oscillations around an initial equilibrium state. The stiffness of the units in such a state varies with an internal self-stress induced by prestretching the cables forming the tensegrity units, and the global prestress induced by the application of compression forces to the terminal bases. The given results show that frequency band gaps of monoatomic and biatomic chains can be effectively altered by the fine tuning of local and global prestress parameters, while keeping material properties unchanged. Numerical results on the wave dynamics of chains under moderately large displacements confirm the presence of frequency band gaps of the examined systems in the elastically hardening regime. Novel engineering uses of the examined systems are discussed.

© 2018 Elsevier Ltd. All rights reserved.

1. Introduction

The research area of linear and weakly nonlinear wave dynamics has devoted much attention to so-called ‘phononic band gap’ theory, which extends the previously investigated theory of photonic band gaps (Lu et al., 2009; Maldovan, 2013; Theocharis et al., 2013; Miniaci et al., 2016a,b; Phani and Hussein, 2017). A number of studies have shown that composite materials that feature periodic variations in density and/or wave velocity can display band gaps where the propagation of mechanical waves is forbidden (refer, e.g., to Phani and Hussein, 2017 and references therein). Structural lattices formed by tensegrity units and lumped masses are particularly interesting for applications. Such systems are easily tunable: either by initial self-stress of the units (also referred to as ‘local’ or ‘internal’ prestress), or by changing the precompression

of the whole structure (‘global’ or ‘external’ prestress, refer to Skelton and de Oliveira, 2010; Fraternali et al., 2012; Fraternali et al., 2014; Fraternali et al., 2015; Amendola et al., 2014; Amendola et al., 2015; Davini et al., 2016; Rimoli and Pal, 2017, and references therein, for an extensive overview).

The research conducted so far in the area of lattice materials alternating tensegrity units and lumped masses has revealed that elastically hardening systems support compressive solitary waves and the unusual reflection of waves on material interfaces (Fraternali et al., 2012; Davini et al., 2016). At the contrary, elastically softening systems support the propagation of rarefaction solitary waves under initially compressive impact loading (Fraternali et al., 2014, 2015; Amendola et al., 2014). Solitary wave dynamics has been suggested for the construction of a variety of novel acoustic devices, like impact mitigation systems and tunable acoustic lenses. Effective impact mitigation systems based on tensegrity systems with softening-type response are able to transform compressive disturbances into solitary rarefaction waves with progressively vanishing oscillatory tail (Fraternali et al., 2015; Herbold and Nesterenko, 2013). Tunable acoustic lenses based on elements

* Corresponding author.

E-mail addresses: adaamendola1@unisa.it (A. Amendola), akrushynska@gmail.com (A. Krushynska), daraio@caltech.edu (C. Daraio), nicola.pugno@unitn.it (N.M. Pugno), f.fraternali@unisa.it (F. Fraternali).

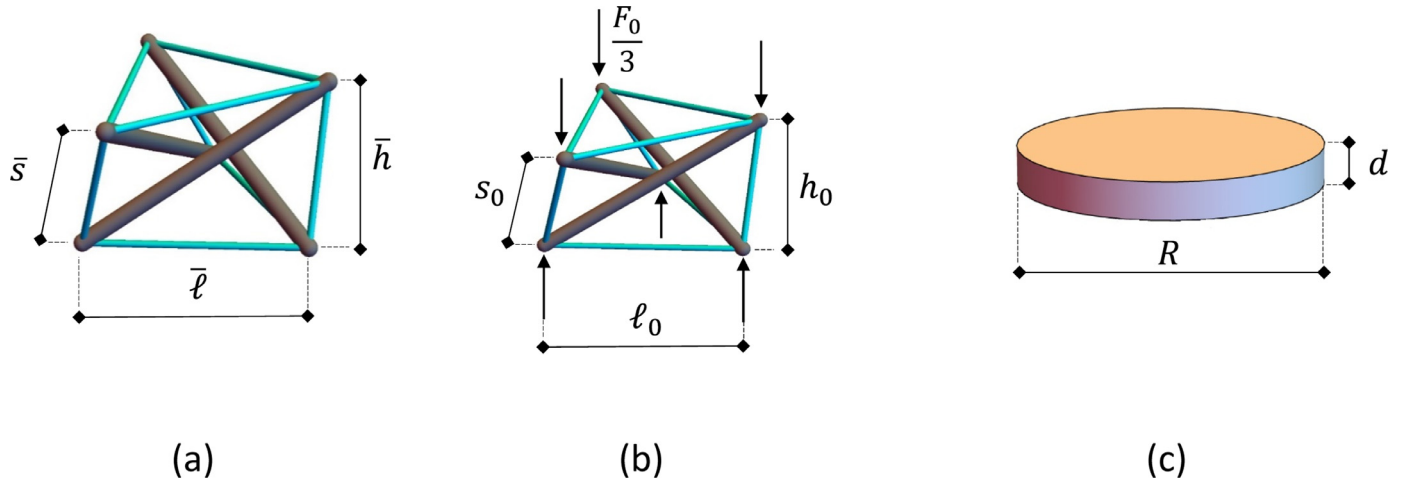


Fig. 1. Rest configuration of a minimal regular tensegrity prism (a), prestressed configuration (b) and lumped mass (c).

with a stiffening response can spatially focus compression solitary waves in different regions of space (Fraternali et al., 2012; Spadoni and Daraio, 2010).

This work investigates translational waves in 1D periodic arrays of tensegrity prisms alternating with lumped masses, which are shown to be able to control linear elastic waves with arbitrary tunable performance starting from (theoretically) zero frequency. The tuning mechanism relies on variability of an effective stiffness of the tensegrity units by means of applied local and global prestress (Fraternali et al., 2012, 2014, 2015; Amendola et al., 2014). We show that such systems support phononic band gaps, which can be tuned to selected frequency ranges by varying the applied prestress, while keeping material properties of the unit cells unchanged. As compared to granular systems (refer, e.g., to Nesterenko, 2001; Theocharis et al., 2013 and references therein), the internal prestress adds a significant extra feature of tensegrity metamaterials, which can be finely tuned in order to essentially vary the system band gaps.

The structure of the paper is as follows: In Section 2 we model the analyzed tensegrity chain as a sequence of masses connected by non-linear springs. We first focus on the linearized mechanical response of a 1D monoatomic lattice (Section 2.1) and then we pass to the analysis of a spring-mass lattice which features springs with two different stiffness constants, as a consequence of different states of local and global prestress (Section 2.2). We show that the dispersion relations of such systems are strongly influenced by the applied levels of prestress. Numerical results obtained in the geometrically nonlinear regime, which accounts for the actual force-displacement response of the tensegrity units under large or moderately large displacements, confirm the presence of frequency band gaps in the dispersion relation of the analyzed systems (Section 3). The key mechanical features of such structures are summarized in Section 4, where we also suggest future research lines for the design and testing of novel band gap systems with tensegrity architecture.

2. Dispersion relation of 1D tensegrity chains

The present section studies the dispersion relation of chains obtained by alternating tensegrity units, acting as elastic springs, and massive discs, acting as lumped masses. The generic tensegrity unit is composed of the minimal regular tensegrity prism illustrated in Fig. 1, which shows two triangular bases composed of members carrying tensile forces (cables or strings), three cross members carrying compressive loads (bars), and three cross-strings.

Table 1

Geometrical and mechanical properties of the rest configuration of the generic unit.

s_N (mm)	l_N (mm)	R (mm)	d (mm)	E_b (MPa)	E_s (MPa)
6.00	8.70	18.66	2.00	120.00	5.48

The chain is uniformly axially loaded by an axial force F (total axial force applied to the terminal bases). We assume that the lattice unit cells are frictionless unilateral contact with the adjacent discs (Fraternali et al., 2014). As such, the bases of the units, being tangentially disconnected from the discs, are free to slide over the surface of these discs. This assumption implies that twisting moments are not transferred from the units to the lumped masses, meaning that the systems examined in the present study do not form continuous 3D tensegrity columns, as opposed to those examined in Krushynska et al., 2018. Accordingly, we describe these systems as 1D chains composed of lumped masses that can move only in the longitudinal direction (Fraternali et al., 2012, 2014), and elastic springs that are characterized by the axial force vs. axial strain response of a uniformly compressed tensegrity prism (Fraternali et al., 2015). We examine chains equipped with tensegrity prisms featuring identical geometrical properties in the rest configuration and identical mechanical properties, with possibly different mechanical response up to the value of the applied prestress.

Hereafter, we use the symbols s , l , and b to denote the current lengths of the cross-strings, the base strings and the bars, respectively, and let h denote the height of the unit. In addition, we let R and d indicate the radius and the thickness of the discs interposed between the units, and make use of the symbols E_b and E_s to denote the Young moduli of the bars and the strings, respectively. The rest lengths of the cross-strings and the base-strings are respectively denoted by s_N and l_N . The units examined in the previous work coincide with those analyzed in Fraternali et al. (2014) for a study on the solitary wave dynamics of tensegrity chains under impact loading. Each unit is composed of 2.28 mm diameter Spectra strings and 0.8 mm diameter cylindrical bars made of the titanium alloy Ti6Al4V. Its rest configuration under zero external and internal forces is described by the properties listed in Table 1. The total mass M of a unit cell is evaluated as the sum of the disk's mass (m) and the prism's mass (m_0). We set $m_0 = 0.083$ g and $m = 24.89$ g, so that the chain can be described as a system of point

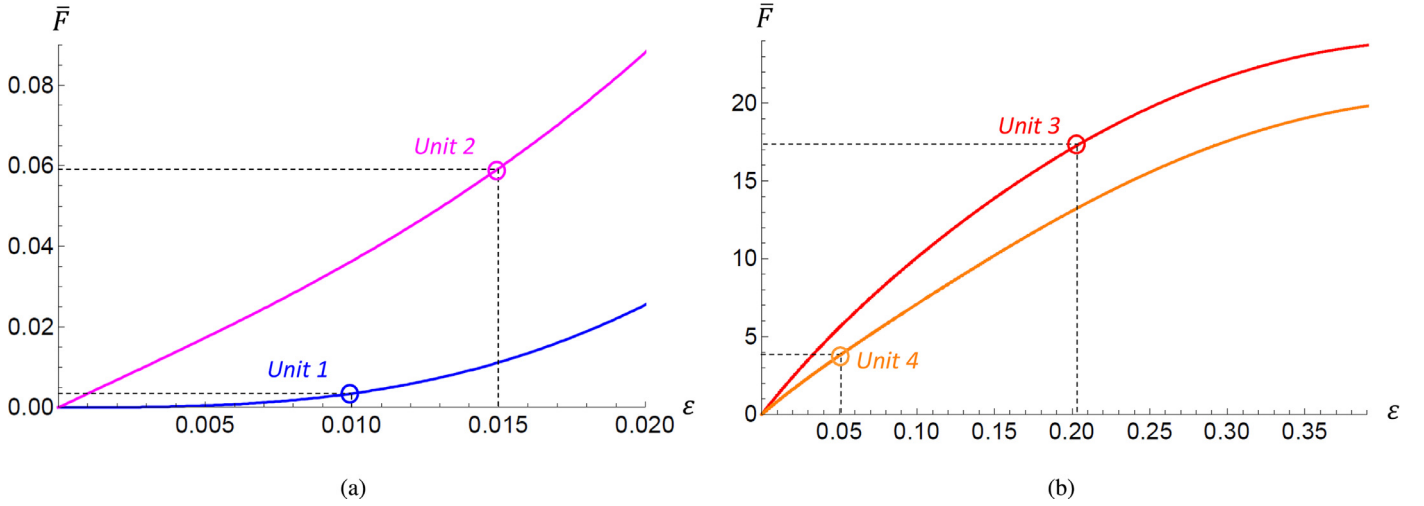


Fig. 2. $F - \varepsilon$ curves of Units 1,2 (a), and 3,4 (b).

Table 2

Variables characterizing the geometry of the self-stressed configuration of the unit under zero external forces, for different values of \bar{p} .

\bar{p}	0.00	0.01	0.02	0.05	0.09	0.10
\bar{s} (mm)	6.000	6.060	6.120	6.300	6.540	6.600
$\bar{\ell}$ (mm)	8.700	8.773	8.845	9.061	9.346	9.417
\bar{b} (mm)	11.108	11.207	11.305	11.597	11.985	12.081
\bar{h} (mm)	5.407	5.463	5.519	5.688	5.913	5.969

masses connected by massless springs ($m \gg m_0$ Fraternali et al., 2014).

Given the action of ‘local’ and ‘global’ states of prestress, let us assume that the generic unit is not in the rest configuration before the application of dynamic loading. A state of local prestress (or self-stress) acts in the configuration of the chain under zero external forces, which shows the two terminal bases of the generic unit rotated against each other at a twisting angle of $5/6 \pi$. This state of prestress follows from the action of a self-equilibrated set of internal forces in the prism members, and can be usefully characterized through the prestrain of the cross-string \bar{p} , as shown in Fraternali et al. (2015) (cf. Table 2).

In addition to local prestress, we assume that the chain is initially loaded with a static precompression force F_0 , which induces a state of global prestress in the structure in the equilibrium configuration preceding the application of dynamic loading. We denote all the quantities referred to the self-stressed configuration by a superimposed dash, and the quantities referred to the globally-prestressed configuration by the subscript ‘0’ (cf. Fig. 1). We let $\delta = \bar{h} - h$ denote the axial displacement from the self-stressed configuration, and let $\varepsilon = \delta/\bar{h}$ denote the corresponding axial strain (positive when the prism is compressed).

The mechanical theory of axially loaded prisms presented in Fraternali et al. (2015) shows that the geometry of an arbitrary configuration of such a structure can be described in terms of three independent geometric variables, say, e.g., the length of the base strings ℓ , the prism height h , and the twisting angle φ between the terminal bases. By using the three equilibrium equation of the generic node, and assuming the linear elastic response of bars and strings, the theory presented in Fraternali et al. (2015) allows us to link ℓ and φ to h (free kinematic variable), and to determine the effective constitutive response F vs. h (or F vs. ε) of the unit, for any couple of values of the variables \bar{p} and $\varepsilon_0 = \delta_0/\bar{h}$ that characterize the local prestress and the global prestress of the unit ($\delta_0 = \bar{h} - h_0$), respectively. Table 3 and Fig. 2 illustrate the geom-

etry and constitutive responses of four units that differ from one another in terms of the values of the prestress variables (\bar{p}, ε_0). In the plots of Fig. 2, the force F has been normalized by introducing the dimensionless quantity $\bar{F} = \frac{F}{(h_0^* + d)K^*}$, where h_0^* is the height and K^* is the tangent stiffness of Unit 1 (taken as reference) in the globally prestressed configuration. The results shown in Fig. 2 reveal that the F vs. ε laws of all the examined units are markedly nonlinear, due to geometric (large displacements) effects. In particular, the \bar{F} vs. ε response of Unit 1 exhibits zero slope at the origin, due to the fact that the unit is under zero local prestress ($\bar{p} = 0$) (Fraternali et al., 2015). It is worth noting that Units 1 and 2 exhibit stiffening tangent response and relatively low tangent stiffness in proximity to the globally precompressed configuration, while Units 3 and 4 exhibit softening response and relatively high tangent stiffness (see Table 3 and Fig. 2).

The study presented in the following Sections 2.1 and 2.2 linearizes the constitutive response of the units near the globally prestressed configuration (ε_0, F_0), by describing such structures as effective linear springs with stiffness constant K equal to the local slope of the $F - h$ curve (tangent axial stiffness). The results presented hereafter are therefore valid for (infinitesimally) small oscillations of the system with respect to the initial configuration. We refer the reader to Section 3 for a study of the dispersion relation of tensegrity chains in the geometrically nonlinear regime.

2.1. Monoatomic chain

Our first goal is to study the band structure of a tensegrity chain by using available results for monoatomic structures (Ashcroft and Mermin, 1976). We analyze a monoatomic tensegrity chain in the form of a sequence of masses connected with linear springs of the same stiffness constant K (Fig. 3). We define the distance between the masses as $H_0 = h_0 + d$, where h_0 is the height of the prism in the initial configuration. The quantity H_0 corresponds to the unit cell size ‘ a ’.

We examine four different monoatomic chains (Mono 1,2,3,4) that respectively employ the Units 1,2,3,4 described in Table 3. In writing the equation of motion of the n th mass forming the chain as follows

$$M\ddot{\delta}_n = K(\delta_{n+1} - \delta_n) - K(\delta_n - \delta_{n-1}) \tag{1}$$

we seek solutions in the form of a propagating harmonic wave

$$\delta_n = Ae^{ikna}e^{i\omega t} \tag{2}$$

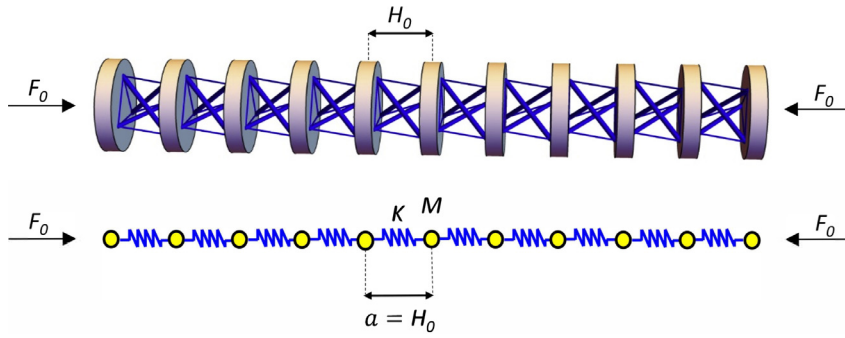


Fig. 3. Monoatomic chain: physical model (top) and mass-spring model (bottom).

Table 3

Geometrical and mechanical properties of four different units, which differ each other for the values of the 'local' prestress variable \bar{p} , and the 'global' prestress variable ε_0 .

	\bar{p} (%)	ε_0 (%)	F_0 (N)	\bar{F}_0 -	s_0 (mm)	ℓ_0 (mm)	h_0 (mm)	a (mm)	ϕ_0 (rad)	K (kN/m)
Unit 1	0.0	1.0	0.0074	0.0035	6.001	8.701	5.353	7.353	2.641	0.395
Unit 2	0.1	1.5	0.125	0.059	6.007	8.709	5.332	7.382	2.652	1.999
Unit 3	5.0	20	36.144	17.097	6.159	9.310	4.551	6.551	2.887	21.652
Unit 4	3.0	5	7.974	3.772	6.148	8.954	5.297	7.297	2.708	26.154

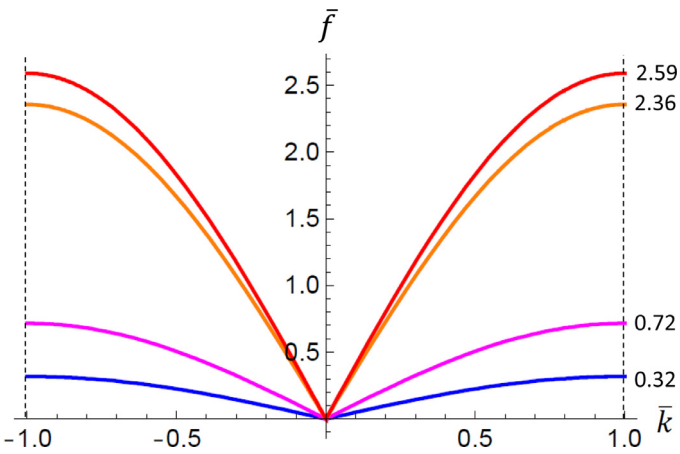


Fig. 4. Dispersion relation in the first Brillouin zone for monoatomic chains equipped with the Units described in Table 3.

where κ is the wave number and ω is the angular frequency (Bloch–Floquet theory, refer, e.g., to Ashcroft and Mermin, 1976). The substitution of Eq. (2) into Eq. (1) leads us to obtain the following single dispersion curve (the so-called “acoustic branch”) between the angular frequency ω and the wave number κ (we refer the reader to Ashcroft and Mermin, 1976 for further details)

$$\omega(\kappa) = \sqrt{\frac{2K(1 - \cos \kappa a)}{M}} \quad (3)$$

Fig. 4 plots the dispersion curves obtained for the four monoatomic chains (Mono 1,2,3,4) following the introduction of the normalized frequency $\bar{f} = f \sqrt{\frac{M}{K}}$ ($f = \frac{\omega}{2\pi}$), and the normalized wavenumber $\bar{\kappa} = \kappa \pi / a$. Let us focus our attention on the end points of the first Brillouin zone ($\bar{\kappa} = \pm 1$), at which the dispersion curve reaches the limiting angular frequency $\omega = \sqrt{\frac{4K}{M}}$, which marks the upper bound of the transmission region of mechanical waves, or, equivalently, the lower bound of the band gap region (band edge) (Ashcroft and Mermin, 1976). The results in Fig. 4 plots point out that mechanical waves with normalized frequencies such that $\bar{f} > 0.32, 0.72, 2.35, 2.59$ (i.e., $f > (40, 90, 296,$

325) Hz) are not allowed to propagate through the Mono1, Mono 2, Mono 3 and Mono 4 chains, respectively. We highlight a $\approx 640\%$ increase of the lower bound of the band gap region, when passing from Mono 1 ($\bar{p} = 0, \varepsilon_0 = 1\%$) to Mono 3 ($\bar{p} = 5\%, \varepsilon_0 = 20\%$), and a $\approx 713\%$ increase of the same quantity when passing from Mono 1 to Mono 4 ($\bar{p} = 3\%, \varepsilon_0 = 5\%$). Therefore, it is clear that one can markedly change the dynamics of mechanical waves in such systems by finely adjusting the local and global prestress of the chain, while keeping unchanged the rest configuration.

2.2. Biatomic chain

We now examine the band structure of a biatomic tensegrity chain (Fig. 5, top), which is modeled by a sequence of identical lumped masses connected by linear springs with alternating constants K_1 and K_2 , where $K_1 < K_2$ (Fig. 5, bottom). The spring with the constant K_1 refers to the 1D model of a tensegrity prism of height ' h_{01} ' at the initial configuration ('soft' unit), while the spring with the constant K_2 refers to a prism of height ' h_{02} ' ('hard' unit).

We define the distance between the two masses connected to the softer prism as $H_{01} = h_{01} + d$. Using the same notation, H_{02} is equal to $h_{02} + d$. Consequently, the unit cell size of the mass-spring model can be defined as $a = H_{01} + H_{02}$ (Fig. 5). As in the case of the monoatomic chain, all the prisms forming the biatomic chain are characterized by identical geometric properties in the rest configuration, as well as identical material properties, and differ only by the value of the local and global prestress (refer to Table 4 for geometric and material properties). By fixing the values of the hard spring constant K_2 and the applied external precompression force F_0 , we study the variation of the mechanical properties of the structure with the soft spring constant K_1 , by examining the units illustrated in Table 4 and Fig. 6.

By extending the Bloch–Floquet theory outlined in the previous section to the case of a biatomic chain, we get a dispersion relation ω vs. κ characterized by the two branches, which are given by the equation (refer, e.g., to Ashcroft and Mermin, 1976; Herbold et al., 2009 for details)

$$\omega^2 = \frac{K_1 + K_2}{M} \pm \frac{1}{M} \sqrt{K_1^2 + K_2^2 + 2K_1 K_2 \cos \kappa a} \quad (4)$$

The lower branch, which is usually referred to as the acoustic branch, covers the frequency range (or pass band) comprised

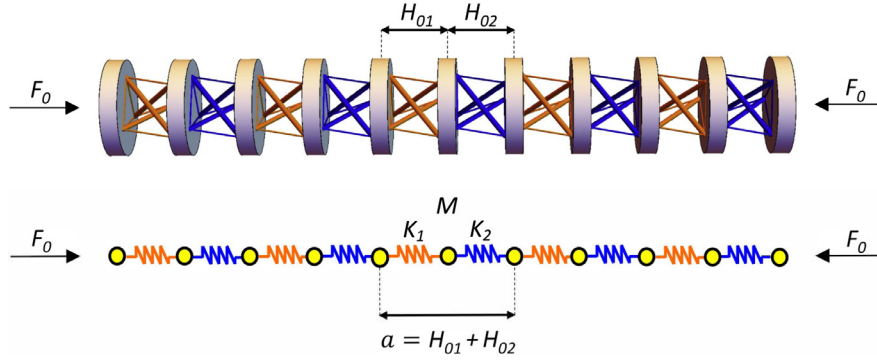


Fig. 5. Biatomic chain: physical model (top) and mass-spring model (bottom).

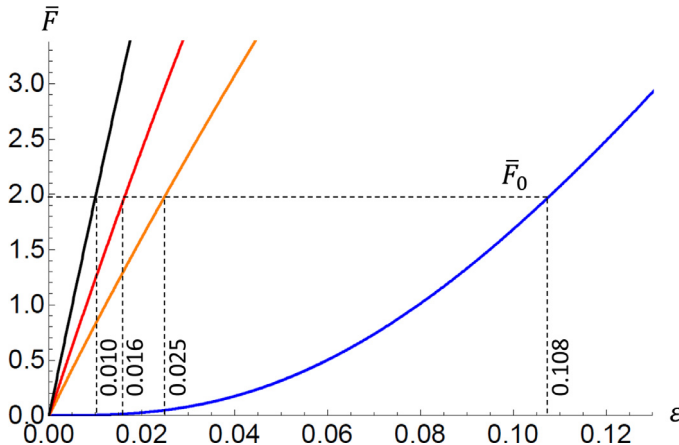


Fig. 6. $F - \varepsilon$ curves of the units of biatomic chains shown in Table 4.

Table 4

Geometrical and mechanical properties of soft and hard units of biatomic chains, for constant $\bar{F}_0 = 1.99$.

	Soft		Hard	
\bar{p}	0.000	0.030	0.050	0.100
ε_0	0.010	0.025	0.016	0.108
K (kN/m)	15.463	28.257	43.107	68.333
s_0 (mm)	6.027	6.161	6.280	6.578
ℓ_0 (mm)	8.776	8.933	9.075	9.430
b_0 (mm)	11.107	11.402	11.597	12.081
h_0 (mm)	4.823	5.436	5.595	5.910

between $\omega = 0$ and $\omega = \sqrt{\frac{2K_1}{M}}$. Likewise, the upper (or optical) branch covers the pass band comprised between $\omega = \sqrt{\frac{2K_2}{M}}$ and $\omega = \sqrt{\frac{2(K_1+K_2)}{M}}$.

Fig. 7 shows the acoustic and optical branches of the dispersion relations obtained for the biatomic chains equipped with the units illustrated in Table 4. The results presented in Fig. 7 highlight that the size of the band gap comprised between the acoustic and optical branches changes markedly when passing from one chain to another, due to the different values assumed by the local and global prestress variables \bar{p} and ε_0 in such systems. By keeping $\bar{p} = 0.100$ and $\varepsilon_0 = 0.010$ in the hard units and varying such prestress parameters in the soft unit, one can get a fixed upper bound at $\bar{f} = 2.96$ ($f = 372.28$ Hz) and tune the lower band gap bound to $\bar{f} = 1.41$ (177.09 Hz), $\bar{f} = 1.90$ (239.40 Hz), and $\bar{f} = 2.35$ (295.68 Hz) when the couple $\{\bar{p}, \varepsilon_0\}$ is respectively equal

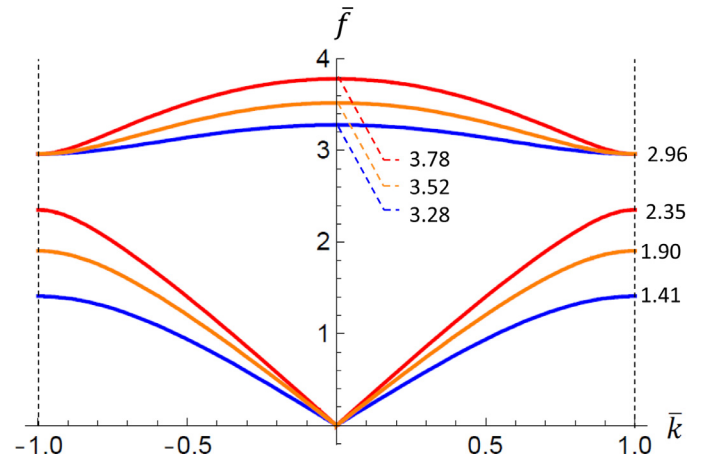


Fig. 7. Dispersion relation in the first Brillouin zone for a biatomic chain under $\bar{F}_0 = 1.99$ and different values of \bar{p} .

Table 5

Geometrical and mechanical properties of the equilibrium points of units equipped with rigid bases under $\bar{F}_0 = 1.17 \times 10^3$.

	Rigel 1	Rigel 2
\bar{p}	0.200	0.000
ε_0	0.076	0.125
K (MN/m)	139.866	540.754
s_0 (mm)	7.782	6.810
ℓ_0 (mm)	8.700	8.700
b_0 (mm)	11.800	11.108
h_0 (mm)	6.201	4.744

to $\{0.000, 0.108\}$, $\{0.030, 0.025\}$, and $\{0.050, 0.016\}$ in the soft units. The above results (Fig. 7) confirm that the band gap frequencies in biatomic tensegrity chains can be effectively tuned by the variation of the local and global prestress, similarly to the monoatomic systems.

The biatomic chains examined in Fig. 7 show band gap frequencies between the acoustic and optical branches within the audible range (20 Hz–20 kHz). This result is a consequence of the particular choice of the prisms and masses forming such systems, and can be generalized to hypersonic band gap system by using, e.g., tensegrity units consisting of prisms equipped with rigid bases and bars (rigid-elastic units Fraternali et al., 2015). Table 5 shows the geometrical and mechanical properties of two rigid-elastic tensegrity units (named ‘Rigel1’ and ‘Rigel2’) that exhibit the same stress-free configuration and identical cross-string ma-

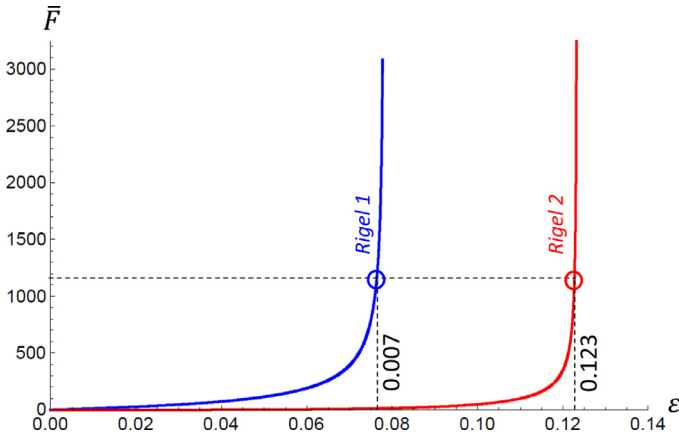


Fig. 8. $F - \varepsilon$ curves of the rigid-elastic units under $\bar{F}_0 = 1.17 \times 10^3$.

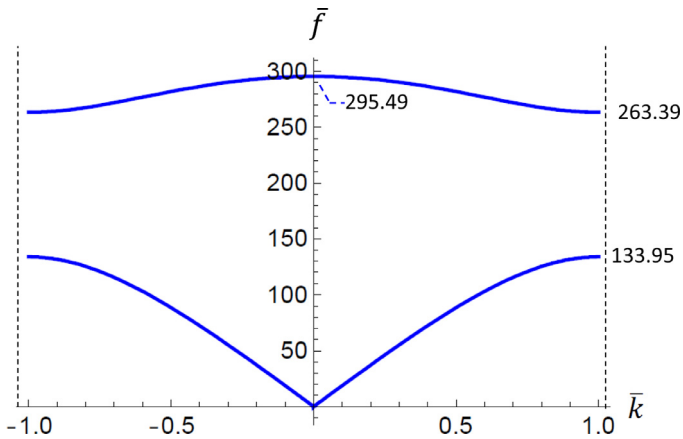


Fig. 9. Dispersion relation in the first Brillouin zone for a biatomic chain equipped with Rigel 1 and Rigel 2 units under $\bar{F}_0 = 1.17 \times 10^3$.

material of the fully elastic prisms previously examined. The axial force vs. axial strain responses of such units illustrated in Fig. 8 highlights a locking-type response in correspondence to the limiting configuration with $\phi = \pi$, when the bars touch each other (Fraternali et al., 2015). The dispersion relation of a biatomic chain equipped with the rigid-elastic units is shown in Fig. 9. It is seen that no waves can propagate along the chain within the first band gap region $\bar{f} \in [133.95, 263.39]$, which extends above the audible frequency range ($f \in [16.84 - 33.12]$ kHz).

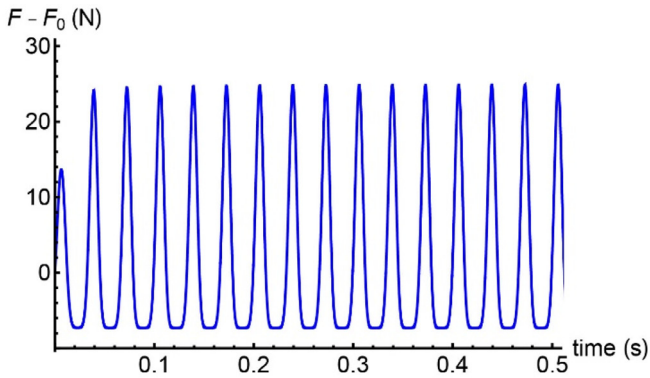
3. Frequency band gaps under moderately large incremental strains

We have already observed that the actual F vs. ε curves of the tensegrity units analyzed in the present work are markedly nonlinear, due to geometric effects (Fraternali et al., 2014, 2015; Amendola et al., 2014) (cf. Fig. 2). We now want to numerically study the phenomenon of wave attenuation in the Mono 1 and Mono 2 chains analyzed in Section 2, by accounting for the nonlinear response of the units under moderately large incremental strains, while varying the values of the local and global prestress variables from $\bar{p} = 0$, $\varepsilon_0 = 1.0\%$ (Mono 1) to $\bar{p} = 0.1\%$, $\varepsilon_0 = 1.5\%$ (Mono 2). Such a study is conducted by perturbing the equilibrium configuration by a sinusoidal time-displacement input applied to the unit #1 of a chain composed of 100 units. The amplitude of the applied displacement input is set equal to 0.03 mm, which gives raise to an incremental strain $|\Delta\varepsilon| \approx 0.6\%$ from the initial equilibrium point

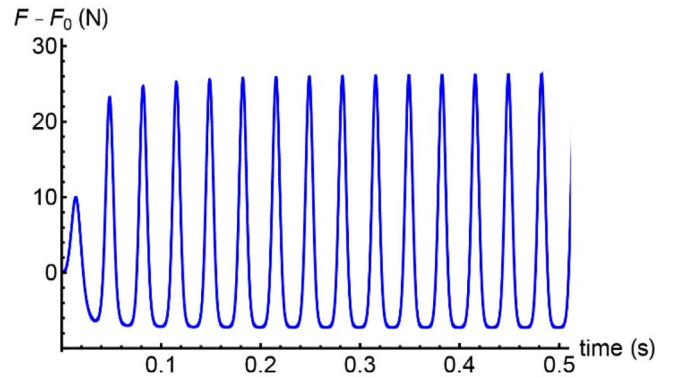
(cf. Table 1), and nearly reduces to zero the static precompression force, when applied in tension (cf. Fig. 2(a)). In the present section, we employ an in-house developed particle dynamics code, which describes the tensegrity units of the Mono 1 and Mono 2 chains as nonlinear elastic springs governed by the force-strain laws depicted in Fig. 2(a). This numerical model makes use of a fourth-order Runge–Kutta integration scheme to solve the Newton equations of motion of the masses forming the chain (see Refs. Fraternali et al., 2012; Ngo et al., 2012; Leonard et al., 2013 for additional details). It differs from that analyzed in Section 2, which studied the Mono 1 and Mono 2 systems as linear mass-spring chains, by linearizing the response of the tensegrity units in proximity to the prestressed configuration.

We begin by analyzing the response of the nonlinear Mono 1 chain. The chain is subjected to sinusoidal displacement loading with excitation frequency $f_{in} \in [20, 80]$ Hz ($\bar{f}_{in} \in [0.16, 0.64]$), thus allowing for the bandgap edge of the linear Mono 1 chain to be included in our analysis ($f = 40$ Hz, implying $\bar{f} = 0.32$, cf. Fig. 4). The given numerical results assume a time integration step equal to $10^{-3}/f_{in}$, which is significantly lower than the oscillation period of the linearized unit ($T_0 \approx 0.003$ s, cf. Ref. Fraternali et al., 2014). Figs. 10 and 11 illustrate the force vs. time outputs for the units 1, 2, 5 and 10 and the fast Fourier transforms (FFTs) of the outputs for units 1, 5, 20 and 50 at excitation frequencies $f = 30$ Hz ($\bar{f} = 0.24$) and $f = 80$ Hz ($\bar{f} = 0.64$), respectively. The FFT results are obtained through the Matlab[®] function ‘fft’ (Version R2017b). The nonlinear response of the analyzed system is clearly visible, since one observes that the output force–time histories $\Delta F = F - F_0$ feature positive peaks larger than the negative peaks, as a consequence of the stiffening-type response of the unit (cf. Fig. 2(a)). The applied excitation induces transient oscillatory pulses ΔF followed by a steady state signal propagating throughout the chain. The latter is characterized by a leading harmonic with frequency f_{in} , and higher-order harmonics of f_{in} , and with reduced amplitude (cf. the (e) panels in Figs. 10 and 11) (Scussel and da Silva, 2016). Fig. 10 shows that the input excitation of frequency $f = 30$ Hz ($\bar{f} = 0.24$) propagates unperturbed through the system (cf. panels (e)–(h)). Differently, Fig. 11 shows that the input disturbance of frequency of $f = 80$ Hz ($\bar{f} = 0.64$) generates a dramatically attenuated output. The ΔF output for $f_{in} = 80$ Hz is indeed very fast reduced in amplitude as it travels along the chain, and progressively vanishes with time already at unit # 2 (cf. panels (a)–(d) of Fig. 11). We observe that the FFT of the ΔF output at unit # 5 exhibits almost zero amplitude for both f_{in} and higher-order harmonics. The FFT plots for $f_{in} = 80$ Hz at the units 5, 20 and 50 feature nearly flat response, with small amplitude, in correspondence to the frequency range below the lower band gap edge of the linear Mono 1 chain (40 Hz). A similar, small amplitude plateau is present also in the FFT of the ΔF output at unit # 1 (not visible in Fig. 11(e) because of its reduced amplitude), and is generated by the transient noisy response of the system.

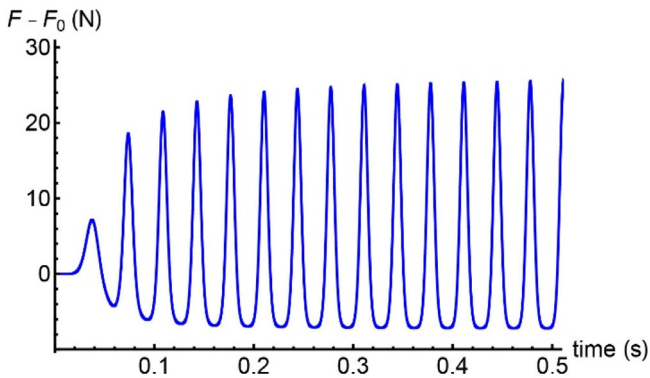
The final Fig. 12 illustrates 3D plots of the FFTs of the ΔF outputs recorded at units # 5 and # 50 of the nonlinear Mono 1 and Mono 2 chains, as the excitation frequency varies from values below the band gap edge of the linear system, i.e., $f = 40$ Hz in Mono 1 ($\bar{f} = 0.32$) and $f = 90$ Hz ($\bar{f} = 0.72$) in Mono 2 (cf. Fig. 4), to values lying above such a threshold. The results in Fig. 12 show that only inputs with excitation frequencies up to the band gap edge of the linear chain are allowed to propagate through the nonlinear systems under consideration. The presence of band gaps in the frequency spectrum is a property of linear systems (cf., e.g., Ref. Herbold et al., 2009). However, we observe that the presence of moderately large incremental strains does not substantially alter the structure of the ‘linear’ dispersion curves shown in Fig. 4, for both the Mono 1 and the Mono 2 chains.



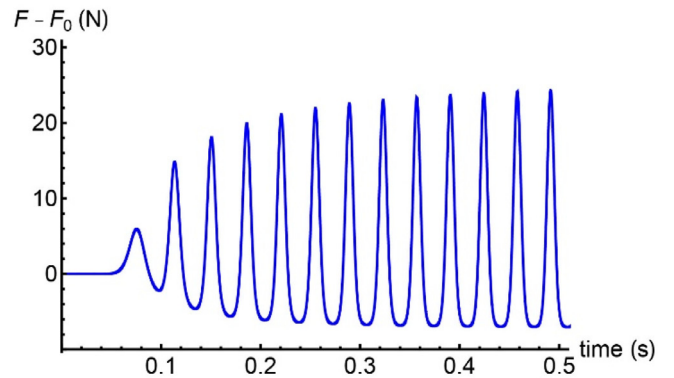
(a) $F - F_0$ unit #1



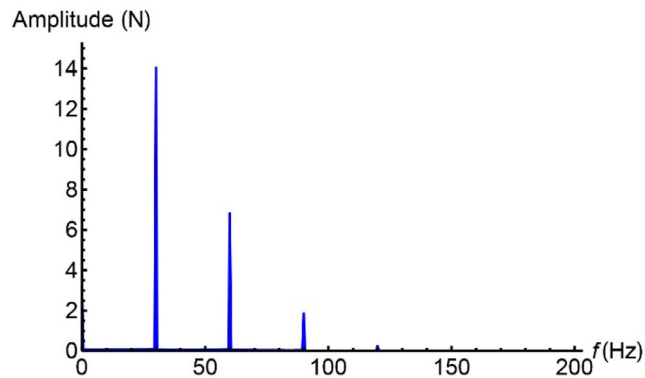
(b) $F - F_0$ unit #2



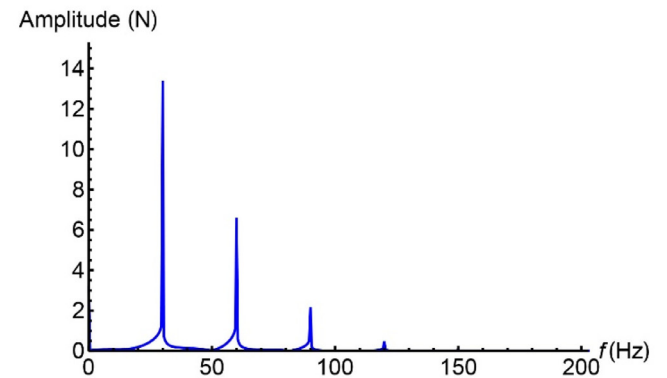
(c) $F - F_0$ unit #5



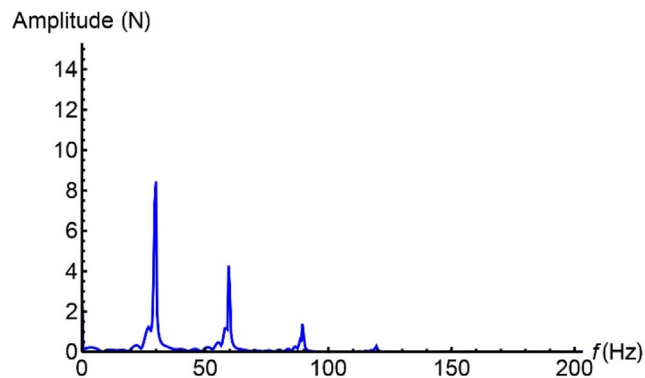
(d) $F - F_0$ unit #10



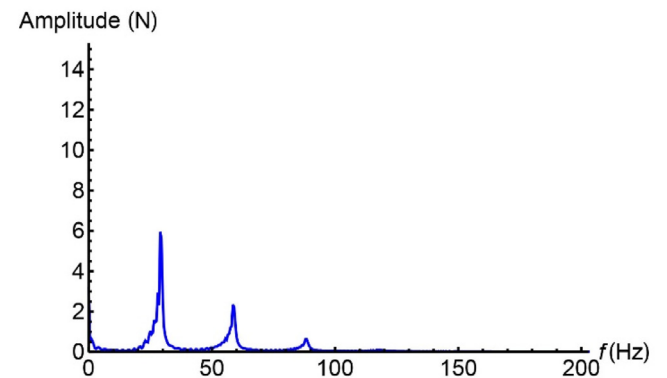
(e) FFT unit #1



(f) FFT unit #5



(g) FFT unit #20



(h) FFT unit #50

Fig. 10. ΔF outputs in units # 1 (a), #2 (b), # 5 (c), and # 10 (d) of the Mono 1 chain, and FFTs of outputs in units # 1 (e), # 5 (f), # 20 (g), and # 50 (h), induced by a sinusoidal time-displacement input with 0.03 mm amplitude and 30 Hz frequency.

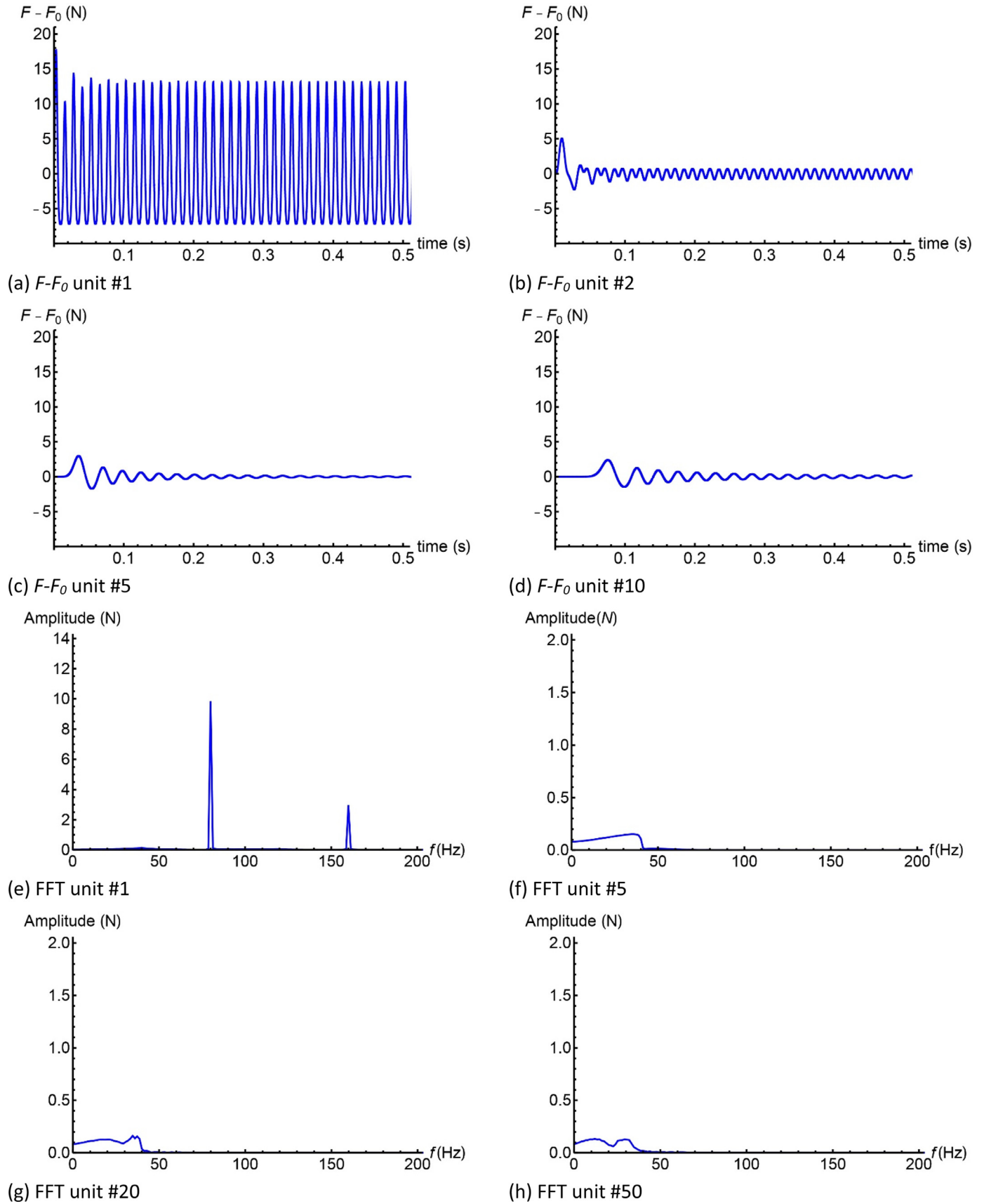


Fig. 11. ΔF outputs in units # 1 (a), #2 (b), # 5 (c), and # 10 (d) of the Mono 1 chain, and FFTs of outputs in units # 1 (e), # 5 (f), # 20 (g), and # 50 (h), induced by a sinusoidal time-displacement input with 0.03 mm amplitude and 80 Hz frequency.

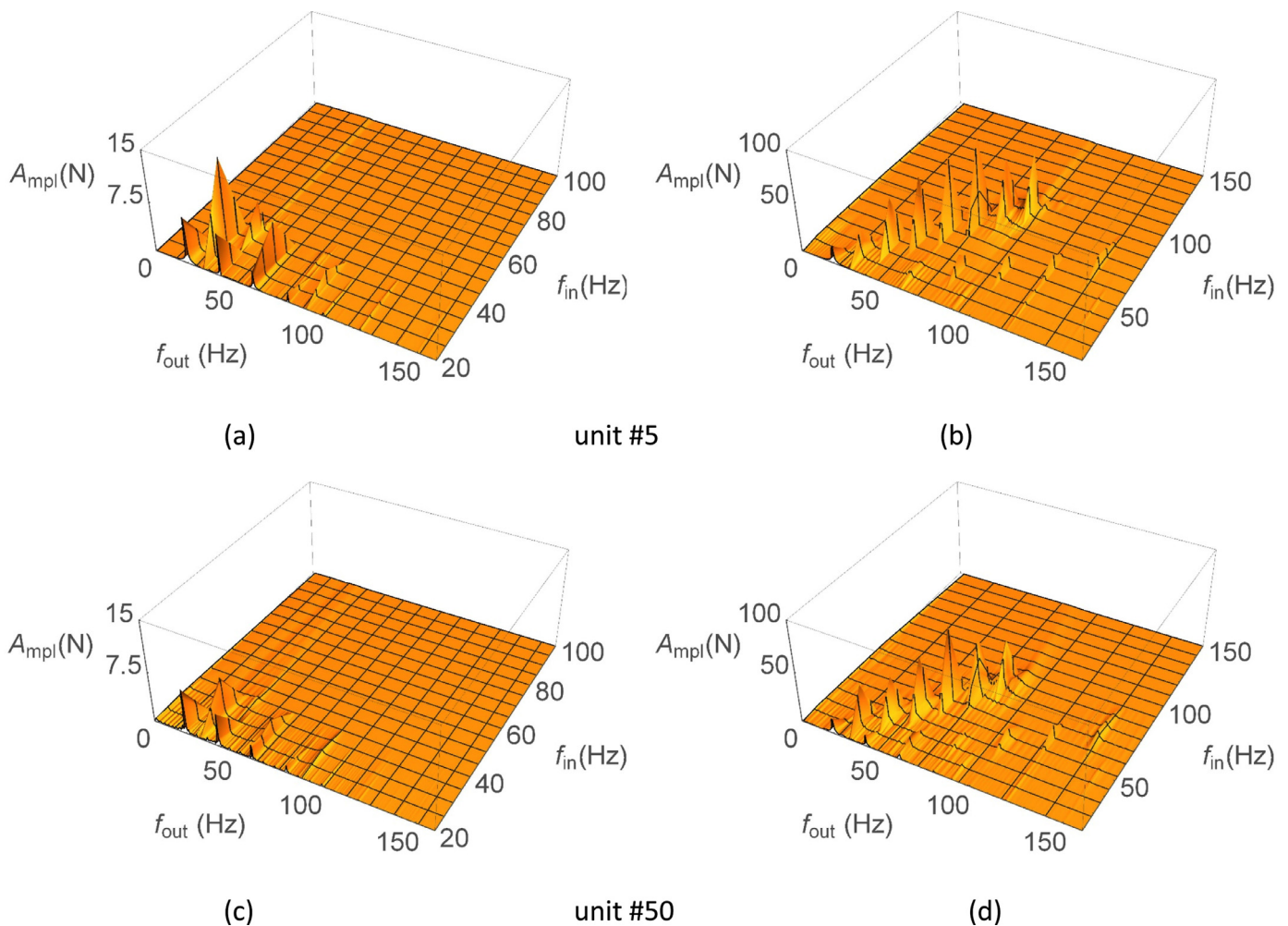


Fig. 12. 3D plots of the FFTs of the outputs recorded in units # 5 and # 50 of systems Mono 1 (left: panels a, c) and Mono 2 (right: panels b, d) under sinusoidal time-displacement inputs with 0.03 mm amplitude and varying excitation frequencies.

4. Concluding remarks

We have analyzed the frequency band structure of 1D tensegrity systems formed by alternating tensegrity prisms with lumped masses. The conducted study assumed constant material properties (eventually accounting for units equipped with rigid bases and bars Fraternali et al., 2015), and variable states of local and global prestress of the system. The results presented in Section 2 have shown that the examined structures exhibit highly tunable frequency band gaps in the linear regime induced by small vibration near the initial equilibrium state, as a function of a parameter \bar{p} describing cable prestretching in the tensegrity unit, and the initial strain ε_0 induced by the precompression applied to the whole system. By suitably varying such parameters it is possible to design monoatomic and biatomic systems that feature band gaps either in the audible and/or in the ultrasonic frequency range (cf. Section 2.2). In Sect. 3 we have generalized these results to the nonlinear regime induced by moderately large incremental strains for a monoatomic system with stiffening-type elastic response. Both the analytic and numerical results presented in Sections 2 and 3 have revealed a novel feature of tensegrity systems, not previously investigated in the to-date literature (see Skelton and de Oliveira, 2010–Rimoli and Pal, 2017 and references therein), which consists of their ability to serve as band gap systems with easily tunable performance, through the control of lo-

cal and global prestress variables, while leaving material properties and the rest configuration of the system unchanged.

The present study paves the way to a number of relevant extensions and generalizations that we address to future work. One natural extension of the current research regards the band structure of lattice materials equipped with multi-atomic bases (Theocharis et al., 2013; Ashcroft and Mermin, 1976), which can be richly designed by alternating tensegrity units equipped with different, material and prestress properties and lumped masses. Such systems may function as band gap systems (Theocharis et al., 2013; Herbold et al., 2009), wave guides (Ruzzene and Scarpa, 2005; Casadei and Rimoli, 2013), impact protection gear (Fraternali et al., 2014, 2010), and/or acoustic lenses (Spadoni and Daraio, 2010; Donahue et al., 2014). Another relevant generalization of the present study regards the modeling of the dispersion behavior of tensegrity systems in the nonlinear regime induced by large strains, to be conducted by recourse to particle dynamics simulations (Herbold et al., 2009), and/or the transfer matrix method (refer, e.g., to Khajehtourian and Hussein, 2014 and references therein). Also the modeling of the dynamical response and control of 3D tensegrity systems deserves special attention (Moored and Barth-Smith, 2009; Zhang and Feng, 2017; Bel Hadj Ali and Smith, 2010; Bel Hadj Ali et al., 2011, 2017), which requires the use of numerical codes dedicated to the dynamics of spatial tensegrity structures (Fabbrocino and Carpentieri, 2017), and/or finite elements simulations (Martin et al., 2010), to account for extensional, twisting and bending modes

(Krushynska et al., 2018), as well as internal resonance phenomena, and edge modes.

Finally, the additive manufacturing and the experimental testing of physical models of tensegrity systems at different scales is a topic of great interest and a challenge at present (Amendola et al., 2015), since it requires the employment of advanced multimaterial deposition techniques that can handle internal prestress. One viable strategy consists of using projection micro-stereolithography setups (Zheng et al., 2012) that employ swelling materials for the tensile members (Lee et al., 2012). Alternatively, one can use multi-jet technologies that handle materials with different coefficients of thermal expansion for struts and cables, in order to create internal self-stress during the deposition process.

Conflict of interests

The authors declare that they have no conflict of interest.

Acknowledgments

AA, FF and NMP gratefully acknowledge financial support from the Italian Ministry of Education, University and Research (MIUR) under the “Departments of Excellence” grant L.232/2016. AOK thanks the funding from the European Union’s 7th Framework programme for research and innovation under the Marie Skłodowska-Curie grant agreement no. 609402-2020 researchers: Train to Move (T2M). CD acknowledges support from the National Science Foundation under EFRI grant no. 1741565. NMP is supported by the European Commission under the Graphene Flagship Core 2 grant no. 785219 (WP14 “Composites”) and FET Proactive “Neurofibres” grant no. 732344.

References

- Amendola, A., Carpentieri, G., de Oliveira, M.C., Skelton, R.E., Fraternali, F., 2014. Experimental investigation of the softening-stiffening response of tensegrity prisms under compressive loading. *Compos. Struct.* 117, 234–243.
- Amendola, A., Hernández-Nava, E., Goodall, R., Todd, I., Skelton, R.E., Fraternali, F., 2015. On the additive manufacturing, post-tensioning and testing of bi-material tensegrity structures. *Compos. Struct.* 131, 66–71.
- Ashcroft, N.W., Mermin, N.D., 1976. *Dynamics of Heterogeneous Materials*, Holt, Rinehart and Winston, New York. ISBN: 8131500527.
- Bel Hadj Ali, N., Rhode-Barbarigos, L., Smith, I.F.C., 2011. Analysis of clustered tensegrity structures using a modified dynamic relaxation algorithm. *Int. J. Solids Struct.* 48 (5), 637–647.
- Bel Hadj Ali, N., Smith, I.F.C., 2010. Dynamic behavior and vibration control of a tensegrity structure. *Int. J. Solids Struct.* 47 (9), 1285–1296.
- Bel Hadj Ali, N., Sychterz, A.C., Smith, I.F.C., 2017. A dynamic-relaxation formulation for analysis of cable structures with sliding-induced friction. *Int. J. Solids Struct.* 126–127, 240–251.
- Casadei, F., Rimoli, J.J., 2013. Anisotropy-induced broadband stress wave steering in periodic lattices. *Int. J. Solids Struct.* 50 (9), 1402–1414.
- Davini, C., Micheletti, A., Podio-Guidugli, P., 2016. On the impulsive dynamics of t3 tensegrity chains. *Meccanica* 51 (11), 2763–2776.
- Donahue, C., Anzel, P.W.J., Bonanomi, L., Keller, T.A., Daraio, C., 2014. Experimental realization of a nonlinear acoustic lens with a tunable focus. *Appl. Phys. Lett.* 104, 014103.
- Fabbrocino, F., Carpentieri, G., 2017. Three-dimensional modeling of the wave dynamics of tensegrity lattices. *Compos. Struct.* 173, 9–16.
- Fraternali, F., Carpentieri, G., Amendola, A., 2015. On the mechanical modeling of the extreme softening/stiffening response of axially loaded tensegrity prisms. *J. Mech. Phys. Solids*, 74, 136–157.
- Fraternali, F., Carpentieri, G., Amendola, A., Skelton, R.E., Nesterenko, V.F., 2014. Multiscale tunability of solitary wave dynamics in tensegrity metamaterials. *Appl. Phys. Lett.* 105, 201903.
- Fraternali, F., Porter, M., Daraio, C., 2010. Optimal design of composite granular protectors. *Mech. Adv. Mat. Struct.* 17, 1–19.
- Fraternali, F., Senatore, L., Daraio, C., 2012. Solitary waves on tensegrity lattices. *J. Mech. Phys. Solids*, 60, 1137–1144.
- Herbold, E.B., Kim, J., Nesterenko, V.F., Wang, S.Y., Daraio, C., 2009. Pulse propagation in a linear and nonlinear biatomic periodic chain: effects of acoustic frequency band-gap. *Acta Mech.* 205, 85–103.
- Herbold, E.B., Nesterenko, V.F., 2013. Propagation of rarefaction pulses in discrete materials with strain-softening behavior. *Phys. Rev. Lett.* 110, 144101.
- Khajetourian, R., Hussein, M.I., 2014. Dispersion relation of a nonlinear elastic metamaterial. *AIP Adv.* 4, 124308.
- Krushynska, A.O., Amendola, A., Bosia, F., Daraio, C., Pugno, N.M., Fraternali, F., 2018. Accordion-like metamaterials with tunable ultra-wide low-frequency band gaps. *New J. Phys.* doi:10.1088/1367-2630/aad354, (arXiv:1804.02188v1).
- Lee, H., Zhang, J., Jiang, H., Fang, N.X., 2012. Prescribed pattern transformation in swelling gel tubes by elastic instability. *Phys. Rev. Lett.* 108 (21), 214304.
- Leonard, A., Fraternali, F., Daraio, C., 2013. Directional wave propagation in a highly nonlinear square packing of spheres. *Exp. Mech.* 53 (3), 327–337.
- Lu, M.H., Feng, L., Chen, Y.F., 2009. Phononic crystals and acoustic metamaterials. *Mater. Today* 12, 34–42.
- Maldovan, M., 2013. Sound and heat revolution in phononics. *Nature* 503, 209–217.
- Martin, A., Kadic, M., Schittny, R., Bückmann, T., Wegener, M., 2010. Phonon band structures of three-dimensional pentamode metamaterials. *Phys. Rev. B* 86, 155116.
- Miniaci, M., Krushynska, A., Movchan, A.B., Bosia, F., Pugno, N.M., 2016a. Spider web-inspired acoustic metamaterials. *Appl. Phys. Lett.* 109, 071905.
- Miniaci, M., Krushynska, A., Bosia, F., Pugno, N.M., 2016b. Large scale mechanical metamaterials as seismic shields. *New J. Phys.* 18, 083041.
- Moored, K.W., Barth-Smith, H., 2009. Investigation of clustered actuation in tensegrity structures. *Int. J. Solids Struct.* 46 (17), 3272–3281.
- Nesterenko, V.F., 2001. *Dynamics of Heterogeneous Materials*. Springer-Verlag, New York.
- Ngo, D., Fraternali, F., Daraio, C., 2012. Highly nonlinear solitary wave propagation in y-shaped granular crystals with variable branch angles. *Phys. Rev. E* 85 (036602), 1–10.
- Phani, A.S., Hussein, M.I. (Eds.), 2017. *Dynamics of Lattice Materials*. John Wiley & Sons, Ltd, Chichester, UK.
- Rimoli, J.J., Pal, R.K., 2017. Mechanical response of 3-dimensional tensegrity lattices. *Compos. Part B-Eng.* 115, 30–42.
- Ruzzene, M., Scarpa, F., 2005. Directional and band gap behavior of periodic auxetic lattices. *Phys. Status Solidi B* 242 (3), 665–680.
- Scussel, O., da Silva, S., 2016. Output-only identification of nonlinear systems via volterra series. *J. Vib. Acoust.* 138 (041012), 1–13.
- Skelton, R.E., de Oliveira, M.C., 2010. *Tensegrity systems*. Springer, Berlin.
- Spadoni, A., Daraio, C., 2010. Generation and control of sound bullets with a nonlinear acoustic lens. *Proc. Natl. Acad. Sci. U.S.A.* 107 (16), 7230–7234.
- Theocharis, G., Boechler, N., Daraio, C., 2013. *Nonlinear Phononic Structures and Metamaterials*. In: Deymier, P.A. (Ed.). *Springer Series in Solid State Sciences, Acoustic Metamaterials and Phononic Crystals*, 173. Springer-Verlag, Berlin-Heidelberg, Germany.
- Zhang, P., Feng, J., 2017. Initial prestress design and optimization of tensegrity systems based on symmetry and stiffness. *Int. J. Solids Struct.* 106–107, 68–90.
- Zheng, X., Deotte, J., Alonso, M.P., Farquar, G.R., Weisgraber, T.H., Gemberling, S., Lee, H., Fang, N., Spadaccini, C.M., 2012. Design and optimization of a light-emitting diode projection micro-stereolithography three-dimensional manufacturing system. *Rev. Sci. Instrum.* 83, 125001.